

BOUNDARY CONDITION OPTIONS FOR CAROTID BIFURCATION ANALYSIS USING DOPPLER VELOCITY MEASUREMENTS

Márton Bence NÉMETH¹, Benjamin CSIPPA², Zsuzsanna MIHÁLY³, György
PAÁL², Péter SÓTONYI³

¹ Corresponding Author. Department of Hydrodynamic Systems, Budapest University of Technology and Economics. Műegyetem rkp. 3., H-1111 Budapest, Hungary, E-mail: mnemeth@hds.bme.hu

² Department of Hydrodynamic Systems, Faculty of Mechanical Engineering, Budapest University of Technology and Economics. Műegyetem rkp. 3., 1111 Budapest, Hungary

³ Department of Vascular and Endovascular Surgery, Semmelweis University Budapest, Városmajor Str. 68, 1122 Budapest, Hungary

ABSTRACT

The common carotid artery (CCA) is a major blood vessel in the neck that bifurcates into the internal (ICA) and external carotid arteries (ECA) where a stenosis (narrowing of the vessel) can occur. Three-dimensional computational fluid dynamics (CFD) analysis of this bifurcation is a standard practice, although it is challenging to prescribe patient specific boundary conditions to approach patient-specific flow conditions. Our aim was to analyze the effect of different boundary conditions to find the most accurate flow conditions that fit the available measured data best.

We conducted CFD simulations on a carotid bifurcation geometry with an ICA stenosis. Six boundary condition groups were analyzed using patient-specific Doppler velocity measurement data at the inlet and both outlets. Three methods were implemented with defined inlet flow rate and either 0 Pa pressure (Basic), Windkessel model, or given flow division (Murray-law) at the outlets. For the other three methods we defined flow rates at two boundaries and a 0 Pa pressure at the third one.

When all the velocity measurements are available, defining two boundary flow rates shows the closest results to the patient-specific data. However, a problem arises from the difficulty of the Doppler measurements on ICA and ECA, which makes the velocity amplitudes to appear higher than expected. Therefore, cross-sectional corrections were implemented to fit the outlet and inlet flow rates while keeping the measured velocity histories.

Our results show that the Murray and Basic methods, while easily available, might exclude carotid-specific flow conditions since downstream flow resistances are not considered. We conclude that a Windkessel-method could produce the most accurate results without forcing outflow conditions.

However, usually unavailable pressure and velocity measurements are necessary for its application.

Keywords: Doppler velocity measurements, Carotid bifurcation, Boundary condition

NOMENCLATURE

A	$[m^2]$	cross-sectional area
C	$[Pa\ s/m^3]$	capacity
D	$[m]$	diameter
K	$[-]$	area ratio
R_d	$[Pa\ s/m^3]$	distal resistance
R_p	$[Pa\ s/m^3]$	proximal resistance
Q	$[ml/s]$	volume flow rate
t	$[s]$	time
v	$[m/s]$	velocity

Subscripts and Superscripts

CCA	at the common carotid branch
ECA	at the external carotid branch
ICA	at the internal carotid branch
avg	spatial mean
norm	normalized value
*	corrected geometry
–	temporal mean

1. INTRODUCTION

Cardiovascular diseases are the leading causes of death in western countries [1] and therefore thoroughly researched in literature. One of the most common types of such diseases is the so-called stenosis, a narrowing of the vessel, which can lead to stroke by occlusion (blocking) of arteries, which supply the brain. Since bifurcations and junctions are more prone to stenosis [2], the carotid bifurcation is a high-risk area, causing it to be the subject of many investigations to identify the effects of vessel

occlusion [3-5]. A common carotid artery can be found on both sides of the neck. It bifurcates into the internal carotid artery (ICA), and the external carotid artery (ECA). The ICA supplies the brain with blood without backflow during the entire heart cycle, therefore its resistance is low. Meanwhile, the ECA is a peripheral artery with higher resistance.

A standard method in research is to investigate the carotid bifurcation with three-dimensional numerical simulations [6-8]. To accomplish this, patient-specific geometry is necessary, which is usually acquired by segmenting computed tomography angiography (CTA) or magnetic resonance angiography (MRA) images. The segmentation method, however, has the inherent problem of subjectivity. This often appears as over-segmentation, which can cause inaccuracies in the geometry and simulation results [9, 10].

Well-defined boundary conditions are also necessary to achieve patient-specific flow conditions. Many methods are used in the literature to solve this problem [11-13], but a general solution has not been found. The difficulty of this task arises from the fact that, in most cases, patient-specific measurement data are not available, limiting the potential boundary conditions. Usually, non-invasive techniques, such as Doppler velocity measurements are used to gain patient-specific data; however, this is also limited because of the difficulty of the ECA and ICA measurements [14].

We investigate the applicability of six selected boundary conditions based on their effect on basic flow conditions. Furthermore, we attempt to offer simple methods to utilize the available measurement data to improve the simulation geometry.

2. METHODS

2.1 Clinical data, geometry

A patient specific geometry was chosen from a series of CTA and Doppler measurements are given by the Dept. of Vascular and Endovascular Surgery of Semmelweis University and the necessary data were anonymised before the described process. The CTA contains the left Common Carotid Artery (CCA) and its bifurcation, and a 68.5 % stenosis is detected on the Internal Carotid Artery (ICA). The degree of stenosis was calculated with the North American Symptomatic Endarterectomy Trial criteria [15]. The CTA image segmentation was completed using itk-SNAP, focusing only on the major arteries: CCA, ECA, ICA. The Vascular Modeling Toolkit (VMTK) was used for surface smoothing and generating the necessary extensions at the inlet and outlets, including the different cross-sectional transitions described in the geometry boundary correction section.

Doppler velocity measurements were performed for the CCA, ICA, and ECA. From the measurement images of the velocity distribution (Figure 1) the

enveloping curve was selected using the image recognition tools of MATLAB. The gained curve is the maximum velocity at the location of the measurement. The maximum velocity waveforms were averaged over multiple heart cycles, to gain a patient-specific velocity waveform for a single (0.85 sec) heart cycle (Figure 2). Doppler images of the respective arterial sections are also created during the measurement, which was used to correct the segmented arterial diameters.

2.2 Geometry boundary correction

CTA image-based segmentation is a subjective method of arterial geometry reproduction since the low resolution of CTA images can lead to uncertainty in the morphological parameters of the artery. This uncertainty generally takes the form of over-segmentation, thus resulting in larger artery diameters [9].

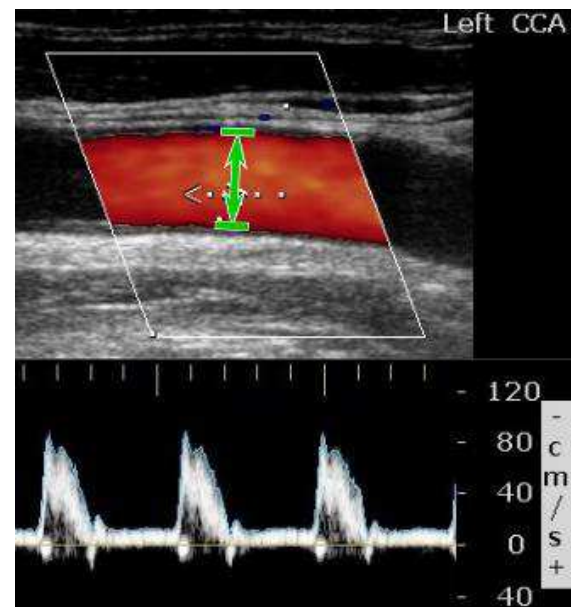


Figure 1. Measured diameter on the Doppler image (top), and Doppler velocity measurement on the CCA (bottom)

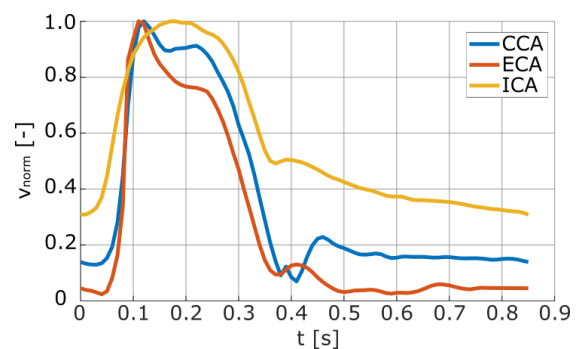


Figure 2. Normalized velocity waveforms of the CCA, ECA and ICA calculated from the Doppler velocity measurements

Two types of geometry modifications were implemented to correct these inaccuracies using patient-specific Doppler measurements.

The CCA cross-section, obtained from CTA images were modified using the Doppler measurement (DCor) images (Fig 1). These images only contain a small section of the arterial geometry, but it is shown in higher resolution than in the CTA. Therefore, in some instances, when an artery can be reliably scanned with the Doppler method, we assumed that its image can be used to measure the diameter of the artery with higher accuracy. We implemented this method to the chosen geometry to approximate the CCA diameter better, correcting the over-segmented (Raw) 42.7 mm² cross-section to 28.0 mm² (Figure 3).

The second geometry modification (QCor) was implemented to achieve a similar correction of the ECA and ICA sections. Since the ECA and ICA branches of the bifurcation are not straight and the change in cross-section is not negligible, Doppler images cannot be used to determine an accurate diameter. However, calculating the flow rate from the velocity shows the necessity of the cross-sectional correction since continuity is not fulfilled. The area ratio K is the ratio between the ECA and ICA outlet areas. We assumed that the segmentation overestimation at the outlet boundaries is proportional to the cross-sectional area. Therefore, the area ratio K is constant, and it is possible to rescale the geometry utilizing the flow continuity. The area ratio K of the outlets in the examined geometry is

$$K = \frac{A_{ECA}}{A_{ICA}} = \frac{A_{ECA}^*}{A_{ICA}^*} = 0.595 \quad (1)$$

where A_{ECA} and A_{ICA} are the cross-sectional areas of the ECA and ICA at the location of the Doppler measurements, respectively before the area correction, while A_{ECA}^* and A_{ICA}^* are the corrected cross-sectional areas. The cross-sectional areas were calculated using the time averaged flow continuity:

$$\bar{Q}_{CCA} = \bar{Q}_{ECA} + \bar{Q}_{ICA} \quad (2)$$

where \bar{Q} is the time-averaged volumetric flow rate. Implementing the K area ratio, the new areas can be calculated as

$$A_{ICA}^* = \frac{A_{CCA} \bar{v}_{avg,CCA}}{K \bar{v}_{ECA} + \bar{v}_{avg,ICA}} \quad (3)$$

where \bar{v}_{avg} is the time and cross-sectional average of the velocities in the respective cross sections.

$$A_{ECA}^* = K A_{ICA}^* \quad (4)$$

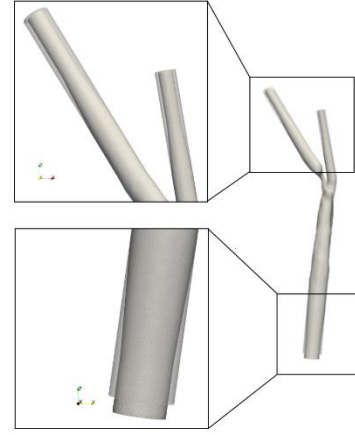


Figure 3. Alteration of the bifurcation geometry produced by the DCOR correction (left) and the QCOR correction (right)

2.3 Boundary conditions

Six boundary condition groups with different measurement data requirements were analyzed during our investigation (Table 1). First, we chose two commonly used methods, where only the CCA velocity data are necessary to define the inlet condition as time-varying volumetric flow rate. Outlet boundary conditions were defined without any additional measurement data necessary. In one case, constant 0 Pascal pressure was defined at the outlets (Basic) with the option to allow backflow [11]. In the other case, a constant ratio of flow division was calculated using the Murray-law (Mur) described by [16]. This flow division method relies on the ratio between the outlet cross-section area and the flow rate of the outlets:

$$\frac{Q_1}{Q_2} = \left(\frac{D_1}{D_2}\right)^3 \quad (5)$$

Therefore, the volume flow ratio had to be recalculated for the geometries where the outlet dimensions were modified.

Three other boundary condition groups were defined utilizing the available outlet velocity measurements. Using the known ECA or ICA velocities, we defined two boundaries as time-varying volume flow, while constant 0 Pa pressure was used at the third one, similar to the Basic method. This created three possible arrangements with at least one outlet having a boundary where the patient-specific flow condition is forced at the given branch (C+E, C+I, E+I).

Last, a three-element Windkessel method (WK3) was implemented at the outlets, with a given volume flow at the inlet. This zero-dimensional model of the downstream system contains a proximal resistance, a distal resistance and a capacity. Aside from velocity measurements, pressure measurements are needed to calculate the patient-specific values of

these constants. Since pressure measurements were unavailable, approximative values were chosen based on [12, 17, 18] to describe the Windkessel-model.

All the boundary condition groups were analyzed for the Raw, DCor, and QCor modified geometries.

Table 1. Inlet and outlet boundary condition definitions

Nr.	Name	Inlet	Outlet
1	Basic	CCA waveform	ECA: Opening ICA: Opening
2	Mur	CCA waveform	Flow rate division
3	C+I	CCA waveform	ECA: Opening ICA: Waveform
4	C+E	CCA waveform	ECA: Waveform ICA: Opening
5	E+I	Opening	ECA: Waveform ICA: Waveform
6	WK3	CCA waveform	3-Element Windkessel-model

2.4 Simulations

In order to gain the volume flow rate values at the inlet and outlets, computational fluid dynamics simulations were carried out. At the carotid bifurcation only low velocities are present, therefore the transient laminar solver of ANSYS CFX was applied for the numerical calculations. As the initial condition of the transient simulations, stationary fluid and zero Pa pressure was defined throughout the volume. To eliminate the effect of the initial condition, three heart cycles were simulated, and only the third cycle was analyzed. To enable transient flow structure generation, the 0.85 sec heart cycles were divided into 5000 times steps, based on the findings of Khan et al. [19].

Triangular surface meshes with 1 million elements were generated for each modified geometry and implemented as rigid walls for the numerical calculations. The effects of the non-Newtonian properties of blood on the flow conditions are considered negligible, therefore we implemented a Newtonian fluid with a density of 1055 kg/m³ and dynamic viscosity of 0.0034 Pas.

In total, 18 setups were simulated for all the possible geometry and boundary group combinations in the present case study.

3. RESULTS

Simulation results of the volume inflow and outflow rate were examined at the third heart cycle. These results were analyzed in four groups based on the similarities in the boundary condition setup.

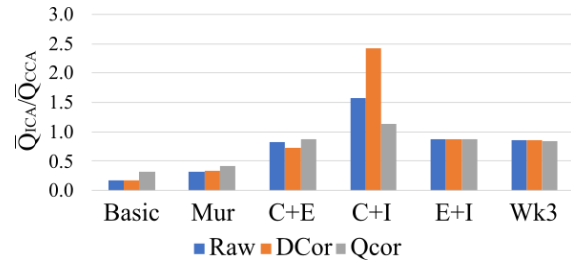


Figure 4. The effect of geometry corrections on volume flow ratio at the different boundary condition groups

Table 2. Main effects of the geometry corrections on the volume flow rate

Nr.	Name	DCor	QCor
1	Basic	Downscaled inlet flow rate	Flow division change
2	Mur	Downscaled inlet flow rate	Flow division change
3	C+I	Downscaled inlet flow rate	Downscaled Q_{ICA}
4	C+E	Downscaled inlet flow rate	Downscaled Q_{ECA}
5	E+I	-	Downscaled Q_{ECA} & Q_{ICA}
6	WK3	Downscaled inlet flow rate	-

3.1 Basic and Murray-law boundary condition groups

Basic and Murray-law simulations resulted in similar volume flow rate waveforms (Figure 5), following the defined Q_{CCA} characteristics. In the Murray-law case, this characteristic is prescribed, while the Basic case produced these results without a forced flow at the boundaries, although the ratio between ICA and ECA differed.

The CCA geometry correction (DCor) resulted in the downscaling of the volume flows since only the Q_{CCA} was decreased via the A_{CCA} reduction (Table 2).

After the second geometry correction (QCor), the volume flow division of the Murray-law was recalculated, producing a more negligible difference between the outlet flow rates, consequently increasing the Q_{ECA} ratio from 0.34 to 0.42. The QCor simulation of the Basic case showed a similar ratio increase from 0.18 to 0.31, as shown in Figure 4.

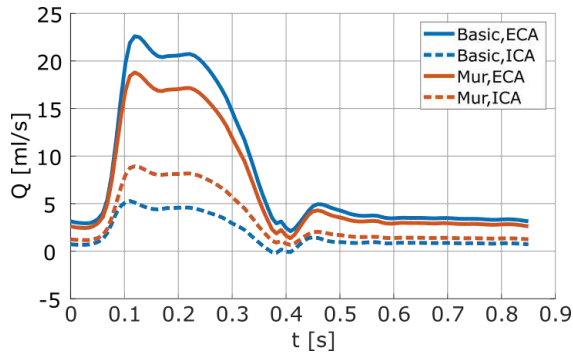


Figure 5. Waveforms of the outlet flow rates between the Basic and Mur boundary condition groups before the geometry corrections

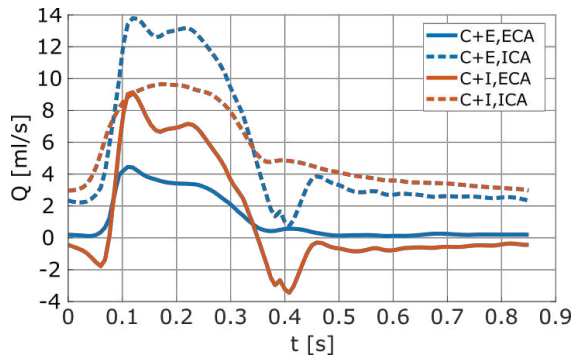


Figure 6. Waveforms of the outlet flow rates between the C+E and C+I boundary condition groups after the QCor geometry correction

3.2 C+E and C+I boundary condition groups

Boundary condition groups where the inlet flow rate and one outlet flow rate are given, produce a flow rate at the other outlet that can be calculated using a continuity equation. Therefore, the geometry correction alters the results only because the flow velocity is the known parameter instead of the volume flow rate.

Ideally, these two boundary condition groups should have the same results since practically all the flow rates are known. However, a clear difference is observable (Figure 6). This difference is the result of a non-simultaneous measurement of the Doppler velocities. In both cases, the volume flow ratio is higher than 0.5, and it stays true after both geometry corrections. This means that $Q_{ICA} > Q_{ECA}$, which could result in a significant velocity increase at the ICA stenosis. In contrast with the previous simulations, the flow rate ratio changes after the first geometry correction, especially at the C+I case from 2.41 to 1.13. The second QCor correction has the opposite effect to the flow division resulting in a similar ratio at the C+E as in the Raw case (0.82 and 0.87) and a lower ratio at C+I (1.58 and 1.13) (Fig. 4).

In the case of the C+I boundary condition group, a flow rate ratio of >1 is observable, which is the equivalent of backflow at the ECA. The Doppler measurements show no such flow condition, however, there are other stenosis cases where backflow is the valid solution.

3.3 E+I boundary condition group

The E+I boundary condition group has a similar setup to the C+E and C+I cases, but the inlet is the 0 Pa boundary instead of one of the outlets. Defining both outlets result in a constant flow rate ratio when the DCor or QCor geometry corrections are applied (Fig. 4). However, the inlet velocity increases with the first correction because of the decreased inlet cross-section. The QCor correction decreases the outlet flow rates and, therefore, the inlet flow rate to a similar average value that was defined in the other boundary conditions based on the CCA Doppler measurements (Figure 7). The average Q_{CCA} is only 1.6 % lower than what can be calculated with the measured velocity and the DCor corrected A_{CCA} , the maximum flow rate differs by 4.8 ml/s and the minimum flow rate differs by 1.8 ml/s. Meanwhile, the flow rate ratio is only 0.96 % lower than in C+I and 28.7 % higher than in C+E in the QCor cases.

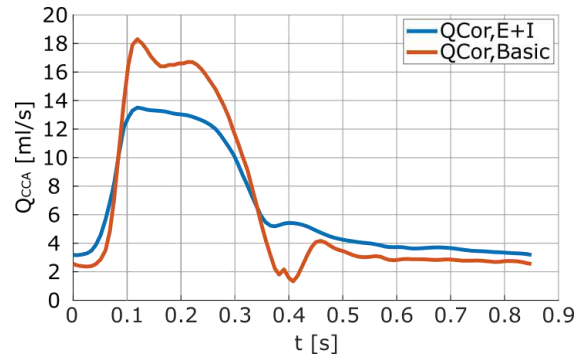


Figure 7. Q_{CCA} waveforms between E+I and Basic boundary condition groups

3.4 Windkessel-method

To calculate the parameters of a three-element Windkessel model, velocity and pressure measurements are necessary. Pressure measurements were not available in our case; therefore, their values were chosen based on the range of values used in the literature (Table 3).

Simulations with the Windkessel model provide a similar flow rate ratio as the E+I option (Fig. 4), with Q_{ICA} being the higher volume flow at the outlets and Q_{ECA} showing temporary backflow. Furthermore, neither the flow rate ratio nor the inflow is sensitive to the Cor and QCor geometry corrections.

Table 3. Approximated values of the 3-element Windkessel parameters

	ECA	ICA
Rp [Pa s/m ³]	10 ⁹	10 ⁸
Rd [Pa s/m ³]	10 ¹⁰	10 ⁹
C [m ³ /Pa]	10 ⁻¹¹	10 ⁻¹⁰

4. DISCUSSION

It is essential to define the boundary conditions correctly because they can significantly affect the flow conditions. At the carotid bifurcation, multiple such boundary condition options are used in the literature [11-13]. While the used boundary conditions are primarily chosen based on the available measured data, some variations can still be accessible. Such variation can be the correction of the inlet or outlet geometries utilizing Doppler imaging to decrease over or under segmentation. In this paper, we investigated the capabilities of 6 different boundary condition groups and the effect of applying two geometry corrections.

At the Murray and Basic methods, the volume flow results are determined by the geometry of the modelled arterial section. This can be seen in their similar waveforms and the effect of the geometry corrections on the flow ratio. While the Murray-law method applies the relation of the cross-sectional diameter and the volume flow rate [16], it does not consider that the resistances of downstream arteries greatly influence the flow conditions at the carotid bifurcation. In our case, these two boundary condition groups underestimated the volume flow at the ICA section compared to the later simulations where the Doppler velocity measurements were applied at the ICA outlet.

The second set of boundary conditions was introduced with C+E, C+I, and E+I, where the volume flow was defined at two boundaries. In these simulations, the flow rate ratio shows that Q_{ICA} is higher than Q_{ECA} . This is the expected flow division since ICA supplies blood to the brain, therefore its demand is expected to be higher [20, 21]. This volume flow ratio is further validated in our case with the Doppler velocity measurements, which show the same effect. Although these three solutions have similar flow divisions, significant differences were observed in the amplitudes and waveforms of the volume flow rate cycle. These differences could be the result of the Doppler measurements not being simultaneous. If the properties of the heart cycle change between the measurements, then the calculated volume flow rates will not fulfil the continuity.

Another problem with the defined outlet is that the Doppler measurements are challenging to perform at the ICA and ECA [14]. For example, if a velocity cycle is measured close to the stenosis, the maximum velocities will appear higher, causing any defined flow rate in that branch to be invalid.

Therefore, these solutions are highly dependent on the accuracy of the measurements. However, if well-executed measurements are available, a patient-specific solution can be achieved by directly forcing the downstream physics at the outlets. While such forced boundary conditions are usually avoided in computational practice, these methods can allow flow conditions that do not develop with the more conventional Basic or Murray-law methods. For example, backflow is possible from the outlets, which can occur in highly stenotic cases [22].

The Windkessel boundary condition applies the physical properties of the downstream arteries, but without forced outlet conditions. With certain values of the WK3 parameters, a backflow condition can also be achieved. The downside of this model is the additional measurements necessary to apply a patient-specific flow condition [17]. This method could provide the most accurate results, but it is rarely accessible for the lack of pressure and velocity data.

The inlet and outlet geometry corrections were implemented based on the idea that a more accurate geometry can be produced from the segmented geometry using the Doppler measurements with novel methods. The results of the corrections are dependent on the used boundary conditions, but in most cases, significant rescaling or flow division change is observable. Since DCor applies the CCA diameter measured from the Doppler image, and QCor applies the outlet diameters based on the measured outlet velocities, the resulting geometry is closer to the actual geometry of the patient. Therefore, the resulting volume flows are a better approximation of patient-specific flow conditions.

The problems with these corrections are similar to the issues of the complex boundary conditions. Namely, it requires additional measurements to calculate the new geometry parameters, and the applicability of these measurements is dependent on their accuracy. In cases where CCA Doppler images are available, a simpler alternative could be to use the DCor method to test the quality of the segmentation. If a significant correction is necessary, it is worth considering resegmentation or additional measurements and application of the QCor method.

It is also essential to note that our investigation only focused on the volume flow results of the simulations. Changes in velocities and wall shear stress could have relevant impacts even at low volume flow changes.

5. SUMMARY

We investigated a single carotid bifurcation with stenosis at the ICA branch, intending to analyze the differences between boundary condition types. To accomplish this, six boundary condition groups were chosen. Furthermore, two geometry correction methods were established utilizing data from Doppler measurements.

We found that boundary conditions without patient-specific outlets are not sufficient at the carotid bifurcation, because they do not consider the resistances of downstream arteries. Other boundary condition setups were implemented with defined velocity waveforms at the outlets to resolve this problem. Although forced flow physics at the outlets is unconventional in practice, these simulations showed closer results to patient-specific conditions. One of the important effects of these setups is the possibility of backflow from an outlet. A three-element Windkessel model was also examined and showed that it produces similar patient-specific conditions without forcing flow physics on the outlets. The drawback of the complex boundary conditions is the additional measurements required and the necessary accuracy of these measurements.

Aside from the boundary conditions, two methods were created to correct the segmented geometry based on the Doppler images and measured velocities. We found that these corrections can significantly affect the amplitude and waveform of the resulting flow rates. The first geometry correction can offer a simple way to test the geometry using the CCA cross-sectional diameter, since the magnitude of the correction is dependent on the inaccuracies of the segmentation. The second correction further improves the geometry in cases where Doppler velocity measurements are available at the outlets without the need of resegmentation.

ACKNOWLEDGEMENTS

This study was supported by the National Research, Development and Innovation Office, under Grant number NKFIH-K 129277 and the Research, Development and Innovation Fund of Hungary under Grant TKP2021-EGA-02.

REFERENCES

- [1] C. J. Murray and A. D. Lopez, "Alternative projections of mortality and disability by cause 1990–2020: Global Burden of Disease Study," *The Lancet*, vol. 349, no. 9064, pp. 1498–1504, May 1997, doi: 10.1016/S0140-6736(96)07492-2.
- [2] R. Ross, "The Pathogenesis of Atherosclerosis — An Update," *New England Journal of Medicine*, vol. 314, no. 8, pp. 488–500, Feb. 1986, doi: 10.1056/NEJM198602203140806.
- [3] J. C. Grotta, "Carotid Stenosis," *New England Journal of Medicine*, vol. 369, no. 12, pp. 1143–1150, Sep. 2013, doi: 10.1056/NEJMc1214999.
- [4] D. Liu, C. Du, W. Shao, and G. Ma, "Diagnostic role of carotid intima-media thickness for coronary artery disease: A meta-analysis," *BioMed Research International*, vol. 2020, Hindawi Limited, 2020. doi: 10.1155/2020/9879463.
- [5] A. M. McKinney *et al.*, "Carotid bifurcation calcium and correlation with percent stenosis of the internal carotid artery on CT angiography," *Neuroradiology*, vol. 47, no. 1, pp. 1–9, Jan. 2005, doi: 10.1007/s00234-004-1301-4.
- [6] S. E. Lee, S. W. Lee, P. F. Fischer, H. S. Bassiouny, and F. Loth, "Direct numerical simulation of transitional flow in a stenosed carotid bifurcation," *Journal of Biomechanics*, vol. 41, no. 11, pp. 2551–2561, Aug. 2008, doi: 10.1016/j.jbiomech.2008.03.038.
- [7] D. Azar *et al.*, "Geometric determinants of local hemodynamics in severe carotid artery stenosis," *Computers in Biology and Medicine*, vol. 114, Nov. 2019, doi: 10.1016/j.compbiomed.2019.103436.
- [8] D. Gallo, D. A. Steinman, P. B. Bijari, and U. Morbiducci, "Helical flow in carotid bifurcation as surrogate marker of exposure to disturbed shear," *Journal of Biomechanics*, vol. 45, no. 14, pp. 2398–2404, Sep. 2012, doi: 10.1016/j.jbiomech.2012.07.007.
- [9] P. Berg *et al.*, "Multiple Aneurysms AnaTomy CHallenge 2018 (MATCH): Phase I: Segmentation," *Cardiovascular Engineering and Technology*, vol. 9, no. 4, pp. 565–581, Dec. 2018, doi: 10.1007/s13239-018-00376-0.
- [10] B. Csippa *et al.*, "Comparison of manual versus semi-automatic segmentations of the stenotic carotid artery bifurcation," *Applied Sciences (Switzerland)*, vol. 11, no. 17, Sep. 2021, doi: 10.3390/app11178192.
- [11] C. J. Lee, N. Uemiya, S. Ishihara, Y. Zhang, and Y. Qian, "A comparison of estimation methods for computational fluid dynamics outflow boundary conditions using patient-specific carotid artery," *Proceedings of the Institution of Mechanical Engineers, Part H: Journal of Engineering in Medicine*, vol. 227, no. 6, pp. 663–671, Jun. 2013, doi: 10.1177/0954411913479540.
- [12] U. Morbiducci *et al.*, "Quantitative analysis of bulk flow in image-based hemodynamic models of the carotid bifurcation: The influence of outflow conditions as test case," *Annals of Biomedical Engineering*, vol. 38, no. 12, pp. 3688–3705, Dec. 2010, doi: 10.1007/s10439-010-0102-7.
- [13] M. Malvè *et al.*, "Impedance-based outflow boundary conditions for human carotid haemodynamics," *Computer Methods in Biomechanics and Biomedical Engineering*, vol. 17, no. 11, pp. 1248–1260, 2014, doi: 10.1080/10255842.2012.744396.
- [14] W. Lee, "General principles of carotid Doppler ultrasonography,"

- Ultrasonography*, vol. 33, no. 1, pp. 11–17, Dec. 2013, doi: 10.14366/usg.13018.
- [15] A. Saxena, E. Y. K. Ng, and S. T. Lim, “Imaging modalities to diagnose carotid artery stenosis: Progress and prospect,” *BioMedical Engineering Online*, vol. 18, no. 1. BioMed Central Ltd., May 28, 2019. doi: 10.1186/s12938-019-0685-7.
- [16] C. Chnafa, O. Brina, V. M. Pereira, and D. A. Steinman, “Better Than Nothing: A Rational Approach for Minimizing the Impact of Outflow Strategy on Cerebrovascular Simulations,” *American Journal of Neuroradiology*, vol. 39, no. 2, pp. 337–343, Feb. 2018, doi: 10.3174/ajnr.A5484.
- [17] I. E. Vignon-Clementel, C. A. Figueroa, K. E. Jansen, and C. A. Taylor, “Outflow boundary conditions for 3D simulations of non-periodic blood flow and pressure fields in deformable arteries,” *Computer Methods in Biomechanics and Biomedical Engineering*, vol. 13, no. 5, pp. 625–640, Jan. 2010, doi: 10.1080/10255840903413565.
- [18] U. Morbiducci *et al.*, “Outflow conditions for image-based hemodynamic models of the carotid bifurcation: Implications for indicators of abnormal flow,” *Journal of Biomechanical Engineering*, vol. 132, no. 9, Sep. 2010, doi: 10.1115/1.4001886.
- [19] M. O. Khan, K. Valen-Sendstad, and D. A. Steinman, “Narrowing the expertise gap for predicting intracranial aneurysm hemodynamics: Impact of solver numerics versus mesh and time-step resolution,” *American Journal of Neuroradiology*, vol. 36, no. 7, pp. 1310–1316, Jul. 2015, doi: 10.3174/ajnr.A4263.
- [20] J. Kochanowicz *et al.*, “Normal reference values of ratios of blood flow velocities in internal carotid artery to those in common carotid artery using Doppler sonography,” *Journal of Clinical Ultrasound*, vol. 37, no. 4, pp. 208–211, May 2009, doi: 10.1002/jcu.20502.
- [21] M. Schöning, J. Walter, and P. Scheel, “Estimation of cerebral blood flow through color duplex sonography of the carotid and vertebral arteries in healthy adults,” *Stroke*, vol. 25, no. 1, pp. 17–22, Jan. 1994, doi: 10.1161/01.STR.25.1.17.
- [22] J. Wang, C. Zheng, B. Hou, A. Huang, X. Zhang, and B. Du, “Four collateral circulation pathways were observed after common carotid artery occlusion,” *BMC Neurology*, vol. 19, no. 1, Aug. 2019, doi: 10.1186/S12883-019-1425-0.